Photochemistry |*Hot Paper*|

Visible-Light Direct Conversion of Ethanol to 1,1-Diethoxyethane and Hydrogen over a Non-Precious Metal Photocatalyst

Yuguang Chao,[a, b] Wenqin Zhang,[a] Xuemei Wu,[a, b] Nana Gong,[a, b] Zhihong Bi,[b, c] Yunqin Li,[a] Jianfeng Zheng,*[a] Zhenping Zhu,[a] and Yisheng Tan*[a]

Abstract: Converting renewable biomass and their derivatives into chemicals and fuels has received much attention to reduce the dependence on fossil resources. Photocatalytic ethanol dehydrogenation–acetalization to prepare value-added 1,1-diethoxyethane and H_2 was achieved over non-precious metal CdS/Ni-MoS$_2$ catalyst under visible light. The system displays an excellent production rate and high selectivity of 1,1-diethoxyethane, 52.1 mmol g^{-1} h^{-1} and 99.2%, respectively. In-situ electron spin resonance, photoluminescence spectroscopy and transient photocurrent responses were conducted to investigate the mechanism. This study provides a promising strategy for a green application of bioethanol.

The conversion of solar energy to electrical and chemical energy has become the hot topic of research recently.[1–10] Converting water into renewable hydrogen (H_2) fuel by photocatalytic water splitting, inspired by natural photosynthesis, has been considered as a promising avenue to settle the energy and environmental issues, attracting enthusiastic attention in recent decades.[11–15] However, a sacrificial agent (e.g., methanol and ethanol) needs to be added to improve the efficiency of solar-to-H_2 conversion in most reaction systems.[16–22] The main function of these sacrificial agents is capturing photogenerated holes to accelerate water oxidation kinetics. Unfortunately, most of the sacrificial agent is oxidized to CO or CO_2, which is harmful to the environment.[23,24] Considering that one of the most important bio-alcohols, ethanol, contains 13.04 wt% of hydrogen, it is perceived as a potential hydrogen

storage medium and is obtained from biomass fermentation.[25] Therefore, photocatalytic ethanol dehydrogenation, converting into value-added chemicals without CO_x release, is a logical strategy to solve the problems outlined above.

1,1-diethoxyethane (DEE), a value-added derivative product of selective ethanol oxidation, has drawn intense attention recently due to its multidisciplinary applications in pharmaceuticals, fuel additives, the fragrance industry and in intermediates for chemical synthesis.[26–28] Particularly, DEE is regarded as a remarkable additive to replace ethanol in fuel because it can keep or increase the cetane number of the fuel[29] and combust the resulting mixtures more drastically.[30] Interestingly, as an additive into fuel, DEE can also significantly inhibit the emission of nitrogen oxide.[31] All these features indicate that the conversion into DEE is a promising channel for the rational utilization of bioethanol. However, the traditional conversion of ethanol into DEE requires two steps: selective oxidation of ethanol to aldehyde and then acid-catalyzed aldehyde-ethanol acetalization to DEE.[31–33] In this traditional approach, the oxidation step is highly damaging to environment and the system is really complex and strict in terms of reactor equipment. Therefore, it is an urgent requirement to apply a simple method to convert ethanol to DEE green and economically.

The photocatalytic acetal reaction supplies a novel strategy to convert ethanol into acetal effectively. Our group achieved visible-light driven methanol dehydrogenation-acetalization, producing 1,1-dimethoxymethane and H_2 over noble-metal-free photocatalyst CdS/Ni$_2$P nanostructured in one step.[34] Zhang and co-workers demonstrated that Pd/TiO$_2$ nanostructures are highly photo-active for the dehydrogenation C—O coupling of ethanol into DEE.[31,35,36] Xu's group reported that the decoration of Pd nanocubes onto TiO$_2$ nanosheets allows simultaneous DEE production and H_2 evolution under ultraviolet light.[37] However, the only ultraviolet light response of TiO$_2$ and the expensive noble metal co-catalysts restrict the large-scale actual application of photocatalytic acetal reactions.

In this work, ethanol is converted into DEE and H_2 over non-precious metals CdS nanorods/Ni-MoS$_2$ nanosheets by photocatalytic dehydrogenation-acetalization under visible light. A small amount of sulfuric acid exists in the reaction system. The acid not only drives the dehydrogenation of ethanol, but also catalyzes the acetalization reaction. The rate and selectively of photocatalytic DEE evolution reaches 52.1 mmol g^{-1} h^{-1} and 99.2%, respectively, while the H^+ concentration is 30 mM. Simultaneously, the trace acid in the reaction system does not corrode the catalyst or glass reactor at all.

[a] Y. Chao, W. Zhang, X. Wu, N. Gong, Y. Li, Prof. J. Zheng, Prof. Z. Zhu, Prof. Y. Tan
State Key Laboratory of Coal Conversion
Institute of Coal Chemistry, Chinese Academy of Sciences
Taiyuan, 030001 (China)
E-mail: zhengjf@sxicc.ac.cn
tan@sxicc.ac.cn

[b] Y. Chao, X. Wu, N. Gong, Z. Bi
University of Chinese Academy of Sciences
Beijing, 100049 (P.R. China)

[c] Z. Bi
Key Laboratory of Carbon Material, Institute of Coal Chemistry
Chinese Academy of Sciences
Taiyuan 030001 (P.R. China)

Supporting information and the ORCID identification number(s) for the author(s) of this article can be found under:
https://doi.org/10.1002/chem.201804664.

These are not the final page numbers! ↗↗
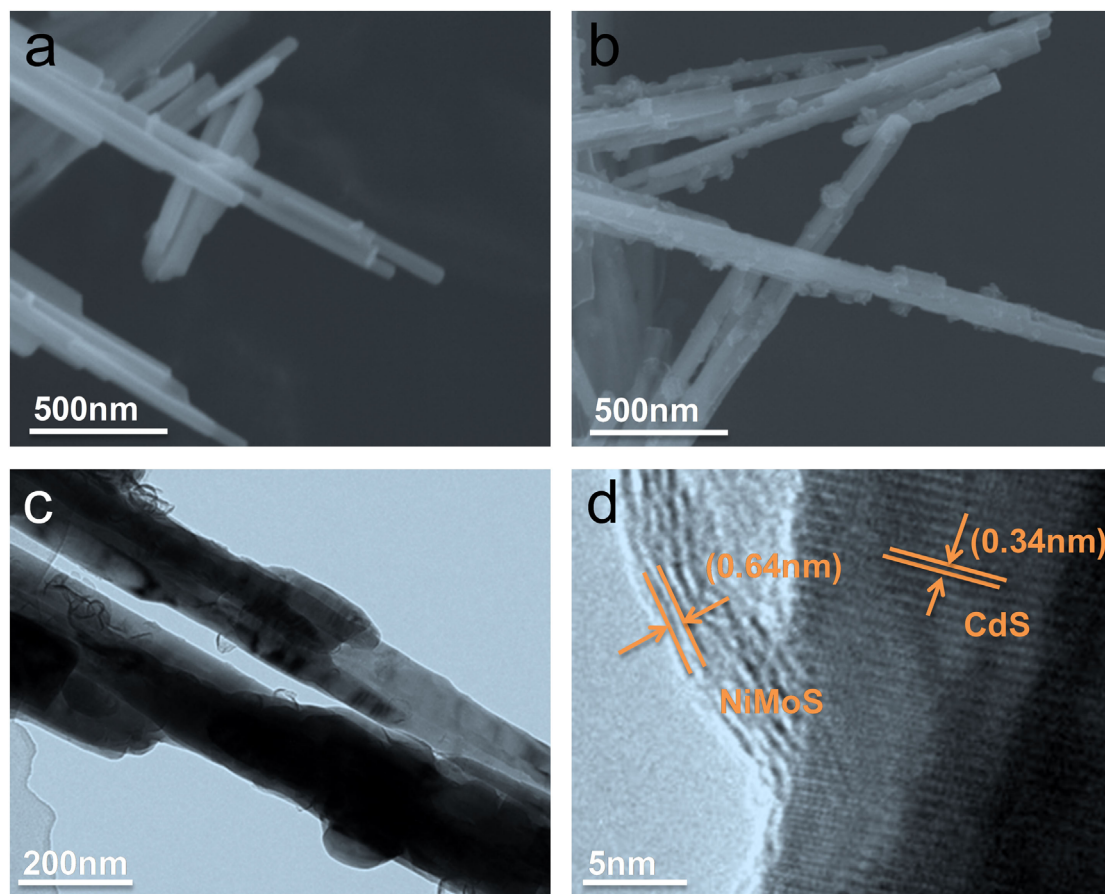
Figure 1. (a) Typical SEM image of blank CdS nanorods, (b) SEM images of as-prepared samples CdS/NiMoS-7 nanostructure. (c) TEM and (d) HRTEM images of as-prepared CdS/NiMoS-7 nanostructure, respectively.

The well shaped CdS nanorods were synthesized on the basis of a previously reported method,[38] and serve as the photocatalyst. The Ni-MoS$_2$ nanosheets were loaded onto CdS nanorods in situ through the solvothermal reaction with L-cysteine, Na$_2$MoO$_4$·2H$_2$O and Ni(NO$_3$)·6H$_2$O as precursors at 200 °C for 30 h. The field-emission scanning electron microscopy (FESEM; Figure 1a and Supporting Information) and transmission electron microscopy (TEM) images (Figure S2a and b, Supporting Information) show that the as-prepared CdS consist of uniform well-shaped 1D nanorods with the average diameter of about 30–40 nm. Figure 1b and c clearly present the FESEM and TEM images of CdS nanorods after growing Ni-MoS$_2$ nanosheets on their surface, and the nanorods kept their 1D geometries. A high-resolution transmission electron microscopy (HRTEM) image (Figure 1d) shows a lattice spacing of about 0.34 nm consistent with the (002) plane of hexagonal CdS, and lattice spacing of about 0.64 nm, coinciding with the (002) plane of Ni-MoS$_2$ nanosheets. X-ray diffraction (XRD) was carried out to investigate the crystal structures of the as-made photocatalysts nanostructure. All characteristic peaks were well in agreement with the standard card of hexagonal CdS (JCPDS card No. 41-1049) (Figure S3, Supporting Information). No obvious diffraction peaks were attributed to Ni-MoS$_2$ in the XRD patterns and no significant diffraction peaks were different from those of the CdS nanorods after the co-catalyst loaded,

probably due to the relatively small amount of Ni-MoS$_2$ distribution and too strong diffraction peaks of the CdS nanorods.[39–41] In addition, we performed the synthesis of Ni-MoS$_2$ without CdS nanorods addition, and the resulting XRD pattern unveiled that the nickel was doped in the MoS$_2$, due to no obvious characteristic peaks of NiS (Figure S4, Supporting Information), which was in agreement with a previous report.[42]

X-ray photoelectron spectroscopy (XPS) was employed for investigating the chemical state of the as-made CdS/Ni-MoS$_2$ nanostructure. The survey scan displayed the existence of Cd, S, Mo, Ni elements in the as-prepared CdS/Ni-MoS$_2$ (Figure S5a, Supporting Information). The binding energy peaks of Mo 3d$_{3/2}$ and Mo 3d$_{5/2}$ were located at 231.4 and 228.2 eV (Figure S5b), respectively, whereas that of S 2p$_{3/2}$ and S 2p$_{1/2}$ peaks were located at 161.1 and 162.4 eV (Figure S5c). These results suggest that the valence states of the Mo and S elements in the final Ni-MoS$_2$ nanosheets were Mo^{4+} and S^{2-}.[43,44] It can be observed from the Ni 2p spectra shown in Figure S5d that the Ni 2p$_{3/2}$ binding energy of 853.4 eV corresponded to the Ni in the Ni-Mo-S structure.[45] The UV/Vis diffuse reflectance spectra (DRS) of the as-synthesized samples are shown in Figure S6, and all the photocatalysts samples gave strong absorption in the region from 200–520 nm, corresponding to the intrinsic band gap absorption of CdS nanorods. Notability, loading the Ni-MoS$_2$ co-catalysts onto the surface of CdS nanorods could

↖↖ These are not the final page numbers!

obviously increase the absorption of samples in the visible-light region of 520–800 nm. This was beneficial to improve the activity of photocatalytic ethanol dehydrogenation.
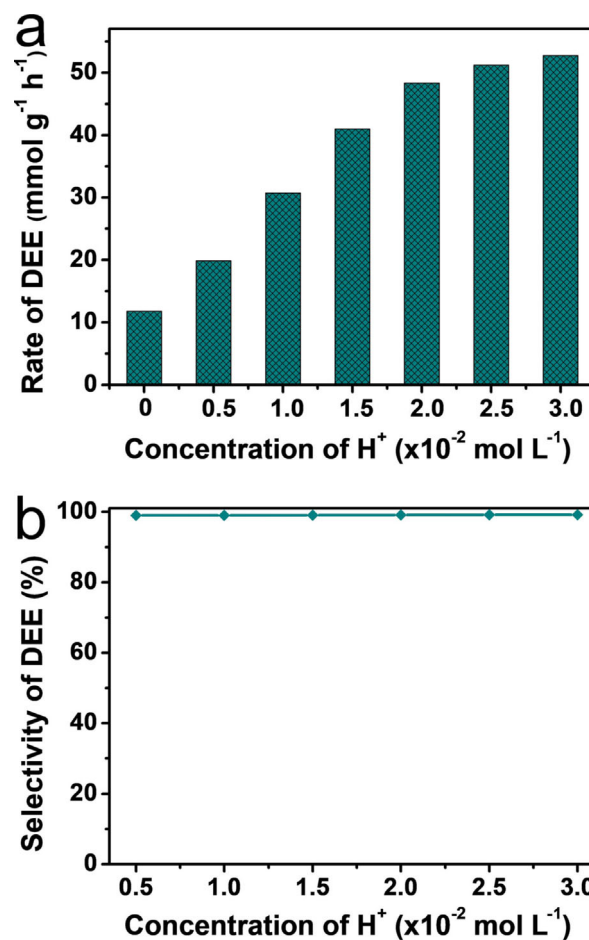
The photocatalytic ethanol dehydrogenation coupling over the CdS/Ni-MoS$_2$ nanocomposites had been performed in ethanol media (containing different concentration of H$^+$) under visible-light irradiation ($\lambda > 420$ nm). Different amounts of co-catalyst Ni-MoS$_2$ nanosheets had been covered on CdS nano-rods to investigate the optimum weight percent of Ni-MoS$_2$ to enhance the photoactivity of catalysts with the concentration of H$^+$ is 30 mM, as shown in Figure 2a. The photocatalytic H$_2$ production exhibited an improved tendency with increasing Ni-MoS$_2$ content. Nevertheless, the excess co-catalyst might reduce the light absorption of CdS nanorods and served as a recombination center for charge carriers, indicating that a suitable co-catalyst content is of importance for optimizing the photoactivity of CdS/NiMoS$_2$.[34] Thereby, the photocatalyst achieved a optimal value at the weight content of 7 wt%, the H$_2$ production rate reaches an optimal value of up to 52.1 mmol g^{-1} h^{-1}, and this result was in accordance with the UV/Vis spectrum (Figure S6, Supporting Information). The dura-

bility of CdS/NiMoS$_2$ catalyst was studied by four consecutive cycles with each cycle of four hours under visible-light irradiation (Figure 2b). At the end of each run, the reactor was evacuated and then refilled with Ar, but the catalyst was not treated. No obvious deactivation was observed within four repeated cycles of photocatalysis and the crystalline structures of CdS/NiMoS$_2$ photocatalyst before and after four cycles had no significant change (Figure S7, Supporting Information), indicating the outstanding photostability of the CdS/NiMoS$_2$ under acidic conditions and the potential for long-term photocatalytic applications.

During photocatalytic H$_2$ evolution from ethanol dissociation, ethanol could be converted into value-added 1,1-diethoxyethane (DEE) in the presence of acid (sulfuric acid). The chemical compositions of the liquid products were analyzed by utilizing GC-MS, as shown in Figures S8 and S9 (Supporting Information). The main liquid phase products were DEE and aldehyde. As H$^+$ played important roles in catalyzing the acetal reaction,[35,46] we investigated the effect with various H$^+$ concentrations on the production rate and the selectivity of DEE. As shown in Figure 3a, the rate of DEE production was increasing with the increase of H$^+$ concentration, and it is worth noting that the rate of DEE production can reach
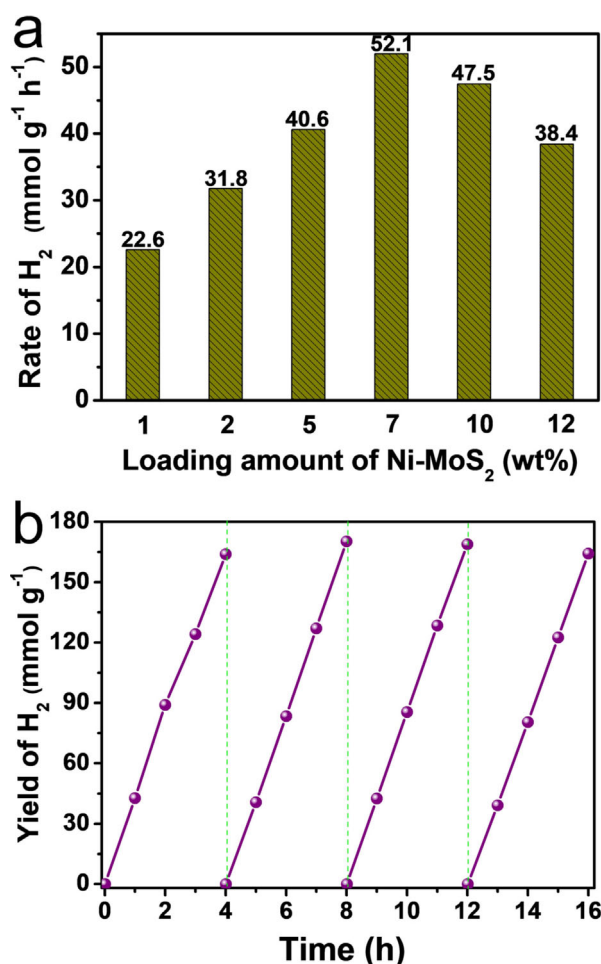

Figure 2. (a) The rates of photocatalytic ethanol dehydrogenation over CdS/Ni-MoS$_2$ samples with different Ni-MoS$_2$ loading amounts [c(H$^+$)$=$40 mM], (b) Photocatalytic ethanol dehydrogenation cycling test (evacuation every 4 h) for CdS/NMS7 samples under visible-light ($\lambda > 420$ nm, 300 W Xe lamp).

Figure 3. (a) The rates of photocatalytic ethanol dehydrogenation at different H$^+$ concentration, (b) The effect of H$^+$ concentration on selectivity of DEE.

These are not the final page numbers! ↗↗

52.1 mmol g^{-1} h^{-1} in 30 mм H$^+$ ethanol solution. However, the selectively had no obvious change at the different H$^+$ concentration (Figure 3 b), which maintains 99.2 %. The high selectively was ascribed to the rapid reaction of ethanol with the product of the dehydrogenation of ethanol in the presence of H$^+$. In addition, the yield of ethanol conversion can reach to 5 % after 12 hours reaction. Interestingly, we did not detect any carbon dioxide in the photocatalysis process, and the only byproduct was aldehyde. Moreover, taking the selectivity of DEE into consideration, the rate of DEE evolution was similar to that of H$_2$, maintaining a ratio of 1:1, indicating the photocatalytic process proceeded nearly by following the chemical equation shown below, also according to the previous report ([Eq. (1)]).[25]

$$3CH_3CH_2OH \xrightarrow[H^+]{h\nu} CH_3-HC\left\langle{{O-CH_2-CH_3}\atop{O-CH_2-CH_3}}\right. + H_2 + H_2O \quad (1)$$
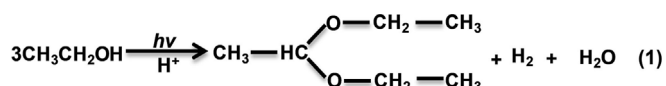
In addition, the effect of acid species added in ethanol solution was also investigated. It is clearly visible that, when the H$^+$ ions were supplied by HCl aqueous solution (36–38 %), both the rate and selectively of DMM production decreased (Figure S10, Supporting Information). The reason was the fast hydrolysis of DEE to acetaldehyde (inverse reaction) in the presence of water, which was introduced by HCl aqueous solution, thus HCl was not an ideal medium to adjust the pH of reaction system.[31,34] Moreover, when no acid was added in the ethanol solution, the rate of photocatalytic H$_2$ evolution decreased sharply and no DEE was detected in the liquid product. The ethanol dehydrogenation and conversion into butane-2,3-diol and aldehyde (Figures S11 and S12, Supporting Information), and the selectivity of butane-2,3-diol and aldehyde were 46.8 and 53.2 %, respectively. This photocatalytic ethanol dehydrated path was consistent with previous reports.[35,47,48] This process also exhibited an excellent photocatalytic H$_2$ evolution stability, having no obvious decrease over 18 h (Figure S13, Supporting Information).

To explore the mechanism of photocatalytic ethanol converting into DEE and H$_2$, an in situ electron spin resonance (ESR) was conducted for the analysis of the reaction intermediates radicals. Figure 4 displays the ESR spectrum during the process of photocatalytic ethanol dehydrogenation coupling reaction by using 5,5-dimethyl-1-pyrroline N-oxide (DMPO, 0.05 м) to capture the reaction intermediates radicals over the CdS/NMS7 photocatalyst. The ESR result shows the existence of hydroxyl ethyl radical ·(CHOHCH$_3$) ($a_N = 15.4$, $a_H = 22$) in the photocatalysis process, which was identical with the Zhang's report.[36] This intermediate should be formed by the dissociation of one H atom from ethanol (α-H) through the oxidation of photo-generated holes. This radical continued to dissociate another α-H by further oxidation, forming one stable aldehyde molecule. Meanwhile, no ethoxy radical was detected, indicating the dehydrogenation occurred at α-H, but not at the O—H. Thus, the value-added DEE could be obtained from the reaction of the generated aldehyde and ethanol under acidic conditions.
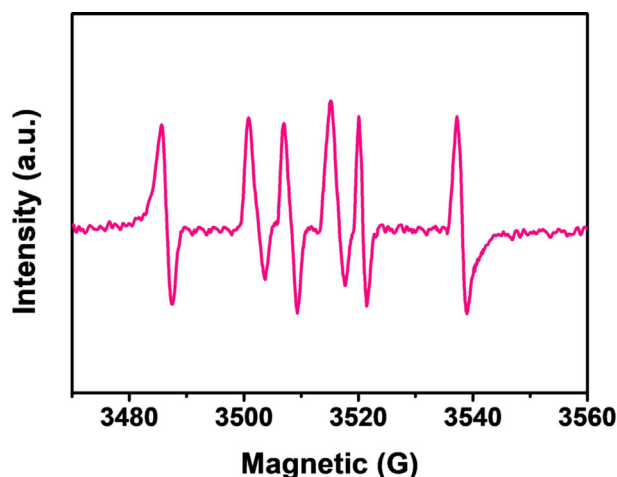

Figure 4. In-situ ESR spectrum in the process of ethanol dehydrogenation over CdS/NMS7 catalyst in the presence of DMPO (a spin-trapping agent) under visible-light irradiation (30 mм H$^+$).

Photoluminescence (PL) spectroscopy and transient photocurrent responses are considered to be powerful techniques for investigating the separation and transfer of charge carriers. Figure 5 a shows two distinct emission bands at about 530 and 640 nm, which could be attributed to near-band-edge emission and the excess of sulfur or core defects on the nanorod surfaces, respectively. The PL emission intensity exhibited an obvious decrease as the co-catalyst Ni-MoS$_2$ loaded, indicating that the co-catalyst Ni-MoS$_2$ can improve the separation efficiency of photo-generated charge carries. Notably, the CdS/NMS7 exhibited the optimal performance to enhance the separation of charge carriers. The transient photocurrent responses were performed with intervals of 10 s periodic light on/off cycles under visible-light irradiation (Figure 5 b). The CdS/NMS7 exhibited the highest cathodic photocurrent among all the as-prepared samples, even twice that of the current of bare CdS nanordos. The addition of co-catalyst Ni-MoS$_2$ accelerated the electron separation and transfer process, resulting in higher performance of photocatalytic ethanol dehydrogenation.

The probable mechanism of visible-light-driven ethanol dehydrogenation-acetalization reaction can be summarized by the above results. CdS nanorods were excited by visible light, producing the photo-generated charge carriers. The electron–holes pairs recombined quickly without the co-catalyst loaded, resulting in relatively poor activity. When Ni-MoS$_2$ was covered on the surface of CdS nanorods, the charge carrier could be separated and transferred effectively. Therefore, the holes on the CdS nanorods were easy to oxidize CH$_3$CH$_2$OH to generate the hydroxyl ethyl radical intermediate, ·CH(OH)CH$_3$. The intermediate was further oxidized to aldehyde (CH$_3$CHO) because of its dynamic instability. Then, the generated aldehyde reacts with ethanol rapidly to form DEE under acidic conditions, whereas no acetic acid was detected and no CO$_x$ was released in this reaction. Meanwhile, the two protons generated then transfer to the surface of the Ni-MoS$_2$ nanosheets, followed by reduction to produce H$_2$ by the photo-generated electrons at the conduction band of the CdS nanorods. Therefore, only
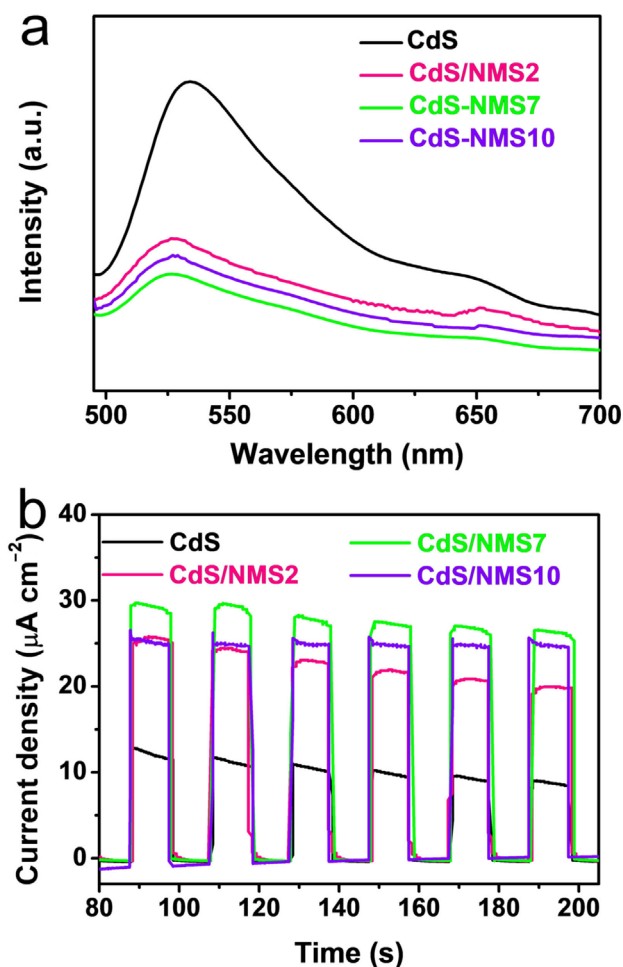
Figure 5. (a) Transient photocurrent responses and (b) photoluminescence spectra with an excitation wavelength of 420 nm of the as-prepared photocatalysts samples.

Conflict of interest

The authors declare no conflict of interest.

value-added DEE and H_2 were generated in this photocatalytic ethanol dehydrogenation-acetalization reaction, avoiding the environmental pollution occurring in traditional acid-catalyzed acetalization processes.

In summary, a photocatalytic ethanol dehydrogenation-acetalization reaction was achieved in one step on non-precious metal catalyst CdS/Ni-MoS$_2$ under visible-light for the first time. The value-added DEE and sustainable H_2 were obtained in this atom-economic green avenue. The optimal photocatalyst CdS/NSM7 composite exhibits excellent rate and selectivity of DEE evolution under suitable acidic conditions ([H$^+$] = 30 mM), which are 52.1 mmol g^{-1} h^{-1} and 99.2%, respectively. There is no CO or CO_2 detected in the gas phase products, avoiding environmental pollution. This work explores a viable strategy for the direct efficient conversion of ethanol into value-added DEE and sustainable H_2 by visible light and provides a promising strategy for green applications of bioethanol.

Acknowledgements

[1] R. Chen, S. Pang, H. An, J. Zhu, S. Ye, Y. Gao, F. Fan, C. Li, *Nat. Energy* **2018**, *3*, 655.
[2] A. Abate, J. P. Correa-Baena, M. Saliba, M. S. Su'ait, F. Bella, *Chem. Eur. J.* **2018**, *24*, 3083.
[3] S. H. Li, N. Zhang, X. Xie, R. Luque, Y.-J. Xu, *Angew. Chem. Int. Ed.* **2018**, *57*, 13082; *Angew. Chem.* **2018**, *130*, 13266.
[4] F. Bella, M. Imperiyka, A. Ahmad, *J. Photochem. Photobiol. A* **2014**, *289*, 73.
[5] A. Sacco, F. Bella, S. De La Pierre, M. Castellino, S. Bianco, R. Bongiovanni, C. F. Pirri, *ChemPhysChem* **2015**, *16*, 960.
[6] G. Zhao, Y. Sun, W. Zhou, X. Wang, K. Chang, G. Liu, H. Liu, T. Kako, J. Ye, *Adv. Mater.* **2017**, *29*, 1703258.
[7] F. Bella, P. Renzi, C. Cavallo, C. Gerbaldi, *Chem. Eur. J.* **2018**, *24*, 12183.
[8] X. Wang, H. Wang, H. Zhang, W. Yu, X. Wang, Y. Zhao, X. Zong, C. Li, *ACS Energy Lett.* **2018**, *3*, 1159.
[9] D. Ompong, J. Singh, *Org. Electron.* **2018**, *63*, 104.
[10] F. Bella, A. Sacco, G. Massaglia, A. Chiodoni, C. F. Pirri, M. Quaglio, *Nanoscale* **2015**, *7*, 12010.
[11] P. Zhou, J. Lai, Y. Tang, Y. Chao, F. Lin, S. Guo, *Appl. Catal. B* **2018**, *238*, 161.
[12] Y. Chao, J. Zheng, H. Zhang, Y. Ma, F. Li, Y. Tan, Z. Zhu, *Energy Technol.* **2018**, *6*, 2132.
[13] N. S. Lewis, D. G. Nocera, *Proc. Natl. Acad. Sci. USA* **2006**, *103*, 15729.
[14] Y. Chao, J. Zheng, H. Zhang, F. Li, F. Yan, Y. Tan, Z. Zhu, *Chem. Eng. J.* **2018**, *346*, 281.
[15] J. Ran, G. Gao, F. T. Li, T. Y. Ma, A. Du, S. Z. Qiao, *Nat. Commun.* **2017**, *8*, 13907.
[16] Y. Honda, H. Hagiwara, S. Ida, T. Ishihara, *Angew. Chem. Int. Ed.* **2016**, *55*, 8045; *Angew. Chem.* **2016**, *128*, 8177.
[17] L. Li, J. Yan, T. Wang, Z. J. Zhao, J. Zhang, J. Gong, N. Guan, *Nat. Commun.* **2015**, *6*, 5881.
[18] C. Xu, W. Yang, Q. Guo, D. Dai, M. Chen, X. Yang, *J. Am. Chem. Soc.* **2014**, *136*, 602.
[19] G. Liu, L. Ma, L.-C. Yin, G. Wan, H. Zhu, C. Zhen, Y. Yang, Y. Liang, J. Tan, H.-M. Cheng, *Joule* **2018**, *2*, 1095.
[20] X. Zhou, E. M. Zolnhofer, N. T. Nguyen, N. Liu, K. Meyer, P. Schmuki, *Angew. Chem. Int. Ed.* **2015**, *54*, 13385; *Angew. Chem.* **2015**, *127*, 13583.
[21] F. Niu, S. Shen, L. Guo, *J. Catal.* **2016**, *344*, 141.
[22] S. Mohajernia, S. Hejazi, A. Mazare, N. T. Nguyen, P. Schmuki, *Chem. Eur. J.* **2017**, *23*, 12406.
[23] J. Saavedra, H. A. Doan, C. J. Pursell, L. C. Grabow, B. D. Chandler, *Science* **2014**, *345*, 1599.
[24] Z. Liu, Z. Yin, C. Cox, M. Bosman, X. Qian, N. Li, H. Zhao, Y. Du, J. Li, D. G. Nocera, *Sci. Adv.* **2016**, *2*, e1501425.
[25] J. C. Serrano-Ruiz, R. Luque, A. Sepulveda-Escribano, *Chem. Soc. Rev.* **2011**, *40*, 5266.
[26] F. Frusteri, L. Spadaro, C. Beatrice, C. Guido, *Chem. Eng. J.* **2007**, *134*, 239.
[27] F. A. J. Meskens, *Synthesis* **1981**, 501.
[28] M. R. Capeletti, L. Balzanob, G. Puente, M. Laborde, U. Sedran, *Appl. Catal. A* **2000**, *198*, L1.
[29] K. Bonhoff, F. Obenaus, Pat. DE, 411, **1980**.
[30] K. Oppenlaender, F. Merger, R. Strickler, F. Hovemann, H. Schmidt, K. Starke, K. Stork, W. Vodrazka, Eur. Pat., 922, **1980**.
[31] H. Zhang, Y. Wu, L. Li, Z. Zhu, *ChemSusChem* **2015**, *8*, 1226.
[32] T. W. Green, *Protective Groups in Organic Synthesis*, Wiley, New York, **1981**.
[33] R. Morrison, R. Boyd, *Organic chemistry, 4th ed.*, Allyn and Bacon, London, **1983**.
[34] Y. Chao, J. Lai, Y. Yang, P. Zhou, Y. Zhang, Z. Mu, S. Li, J. Zheng, Z. Zhu, Y. Tan, *Catal. Sci. Technol.* **2018**, *8*, 3372.

[35] H. Zhang, Z. Zhu, Y. Wu, T. Zhao, L. Li, *Green Chem.* **2014**, 4076.

[36] H. Zhang, W. Zhang, M. Zhao, P. Yang, Z. Zhu, *Chem. Commun.* **2017**, *53*, 1518.

[37] B. Weng, Q. Quan, Y.-J. Xu, *J. Mater. Chem. A* **2016**, *4*, 18366.

[38] J. S. Jang, U. A. Joshi, J. S. Lee, *J. Phys. Chem. C* **2007**, *111*, 13280.

[39] B. Han, S. Liu, N. Zhang, Y.-J. Xu, Z.-R. Tang, *Appl. Catal. B* **2017**, *202*, 298.

[40] S. Cao, Y. Chen, C.-C. Hou, X.-J. Lv, W.-F. Fu, *J. Mater. Chem. A* **2015**, *3*, 6096.

[41] H. Park, D. A. Reddy, Y. Kim, S. Lee, R. Ma, T. K. Kim, *Chemistry* **2017**, *23*, 13112.

[42] Y. Chao, J. Zheng, J. Chen, Z. Wang, S. Jia, H. Zhang, Z. Zhu, *Catal. Sci. Technol.* **2017**, *7*, 2798.

[43] W. Lai, Z. Chen, J. Zhu, L. Yang, J. Zheng, X. Yi, W. Fang, *Nanoscale* **2016**, *8*, 3823.

[44] Z. Yang, D. Gao, J. Zhang, Q. Xu, S. Shi, K. Tao, D. Xue, *Nanoscale* **2015**, *7*, 650.

[45] W. Park, J. Baik, T.-Y. Kim, K. Cho, W.-K. Hong, H.-J. Shin, T. Lee, *ACS Nano* **2014**, *8*, 4961.

[46] T. Simon, N. Bouchonville, M. J. Berr, A. Vaneski, A. Adrovic, D. Volbers, R. Wyrwich, M. Doblinger, A. S. Susha, A. L. Rogach, F. Jackel, J. K. Stolarczyk, J. Feldmann, *Nat. Mater.* **2014**, *13*, 1013.

[47] H. Lu, J. Zhao, L. Li, L. Gong, J. Zheng, L. Zhang, Z. Wang, J. Zhang, Z. Zhu, *Energy Environ. Sci.* **2011**, *4*, 3384.

[48] P. Yang, J. Zhao, B. Cao, L. Li, Z. Wang, X. Tian, S. Jia, Z. Zhu, *ChemCatChem* **2015**, *7*, 2384.
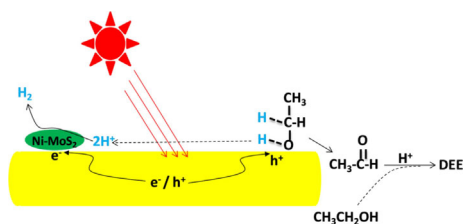
↖↖ These are not the final page numbers!

Remove hydrogen and acetalize: Photocatalytic ethanol dehydrogenation–acetalization to prepare value-added 1,1-diethoxyethane and H$_2$ was achieved over non-precious metal CdS/Ni-MoS$_2$ catalyst under visible light. This work provides a promising strategy for a green atom-economic application of bioethanol.

These are not the final page numbers! ↗↗